IAC-23-C2.9.2

CARBON COMPOSITE STRUCTURES WITH EMBEDDED FIBER OPTIC SENSORS: A SMART PROPELLANT TANK FOR FUTURE SPACECRAFT AND LAUNCHERS

Ahmed E. S. Nosseir[ab]*, Emanuele Alberto Slejko[c], Angelo Cervone[d], Claudio Oton[a], Fabrizio Di Pasquale[a], Stefano Faralli[a]

[a] *Scuola Universitaria Superiore Sant'Anna di Pisa, Institute of Mechanical Intelligence. Via G. Moruzzi 1, 56124 Pisa PI, Italy.*

[b] *University of Trento, Department of Physics, DIN Space Science and Technology. Via Sommarive, 14, 38123 Povo, Trento TN, Italy.*

[c] *University of Trieste, Department of Engineering and Architecture. Via Alfonso Valerio 6, 34127 Trieste TS, Italy.*

[d] *Delft University of Technology (TU Delft), Faculty of Aerospace Engineering. Kluyverweg 1, 2629 HS Delft, Netherlands.*

* Corresponding Author: ahmed.nosseir@santannapisa.it; ahmed.nosseir@unitn.it

Abstract

Modern spacecraft systems and launch vehicle design is more oriented towards reducing system-level design and assembly complexities. In order to maintain high overall system performance while reducing these complexities, the use of smart materials and smart structural components is becoming of more interest to space systems' designers. The paper will present a concept of smart space structures, in particular carbon fiber composites embedded with Optical Fiber Sensors (OFS) for spacecraft and launch vehicle applications. Although the application is of interest as well to electric and hybrid propulsion with suitability for a variety of relevant propellants, the case study presented is on smart propellant tanks to be used in launch vehicle's upper-stage chemical propulsion, utilizing gaseous and liquid fluids with specific interest in green propellants (i.e., EIL and NOx classes). This study will discuss the typical mission and operational requirements for such tanks and the smart features enabled by the optical fiber sensors. For the latter aspect, a quantitative comparison between Fiber Bragg Grating sensors (FBGs) and Distributed Optical Fiber Sensors (DOFS) based on Optical Frequency Domain Reflectometry (OFDR) is presented to highlight their core performance parameters, such as the sensing range and spatial resolution. The proposed smart tanks utilizing optical fiber sensors are found to be capable of providing precise readings of static and dynamic strain as well as temperatures on a wide range. The increased performance and reliability come with a reduction in size, mass, and power consumption compared to the conventional electronic sensors. Optical fiber sensors embedded in carbon fiber structures have proved capability in providing accurate real-time measurements of temperature and monitoring structural integrity while detecting precisely possible points of rupture and failure. The applications of fiber optic sensing in smart propellant tanks may extend to detecting fluid leakage and providing increased precision in propellant gauging and can be used in on-ground qualification, pre-flight testing, as well as in-orbit operation and health monitoring.

Keywords: Advanced Space Systems; Propulsion System; Structural Health Monitoring; Optical Fiber Sensors; Smart Structures.

Nomenclature

n_{eff} effective refractive index
$\Delta\varepsilon^{tot}$ total strain change due to mechanical and thermal effects
ε^{mech} mechanical strain
ε^{th} thermal strain
k a shearing-stress transfer parameter
r_f, r_i, r_m radii of fiber core, interlayer, matrix
p_{11}, p_{12} components in the strain-optic tensor

Acronyms/Abbreviations

OCM – Operations and Condition Monitoring
SHM – Structural Health Monitoring
FBG – Fiber Bragg Grating
OFS – Optical Fiber Sensors
Q-DOFS – Quasi Distributed Optical Fiber Sensors
DOFS – Distributed Optical Fiber Sensors
WDM – Wavelength Division Multiplexing
TDM – Time Division Multiplexing
OFDR – Optical Frequency Domain Reflectometry
OTDR – Optical Time Domain Reflectometry
SoI – Silicon on Insulator
PIC – Photonic Integrated Circuits
TCS – Thermal Control System

1. Introduction

Spacecraft propellant tanks design and manufacturing have ever attracted a keen attention in rocket propulsion

and aerospace structures engineering activities due to their often multi-purpose use as load bearing structures besides their fluid containment and propellants management purposes. The evolution of the production manufacturing processes played the most important role in the performance increase of these structures through reducing their dry mass while increasing or at least maintaining their load bearing abilities.

Propellant tanks, especially those incorporating smart features of operation control, condition monitoring, and health monitoring, evolved to represent a complex subsystem of the propulsion system and the structural system of spacecraft that requires the involvement of interdisciplinary activities of research and development associated to advanced space systems and manufacturing technology [1].

A smart propellant tank would typically be required to provide real-time condition assessment and monitoring of both the contained fluids state and the structural integrity. Parameters of interest to spacecraft operators are fluid temperature, pressure, gauging level and fluid quantity, mass flow rate, as well as fluid state, density, and perhaps viscosity. By increasing the number of measurands and intending higher accuracy, the complexity of the system increases, and most importantly this comes with additional burdens indirectly on the propulsion overall performance degradation accounting for the additional size and mass of the monitoring system required.

Carbon composite are key material allowing the manufacturing of new generation of spacecraft propellant tanks, that will enhance performance and reduce costs, employing new architectures and functions especially those related to Operations and Conditions Monitoring (OCM) of the tanks as a part of the propulsion system as well as the Structural Health Monitoring (SHM) of the tanks as a part of the structural system of the spacecraft.

European Space Agency (ESA) has contracted several European industrial entities to develop the so-called "Black-Stage" launcher stages of the Ariane 6 launch vehicle that is believed to provide significant increase in the payload-to-orbit performance by up to 2000 kg [2] [3].

Nowadays in space propulsion, the industry – seeking as usual the increase of systems' performance and the reduction of costs – needs to further reduce the systems' complexity and lead-time to market through the employment of new technologies particularly those enhancing monitoring and control of subsystems. The monitoring and control systems design relies on sensing technology, data acquisition and processing, and acting towards controlling the system through the decision-making process. Diagnosis and prognosis processes are then enabled by accurate onboard monitoring and control

activities. Typical designs of spacecraft systems and subsystems require the integration of standalone equipment such as temperature and pressure transducers, heating elements and thermal control devices and strain measurement sensors, among others. Each of these components require dedicated design review process and validation procedures in addition to more hardware and logistics costs which adds burdens to the project life cycle. Moreoever, integration of separate components to create a monitoring system implies increased risk of inaccuracies which eventualy degrades the precision of the acquired data thus affecting the analysis and the decision making for the control activities.

Smart structures and advanced space systems would play an important role in addressing the above mentioned concerns and acting towards the increase of systems' performance, cost reduction, and complexities handling. A Smart Propellant Tank design envisage employing embedded sensors of several types, such as Optical Fiber Sensors (OFS), thin-film sensors, and piezo electric sensors to enable highly accurate and precise real-time operations and condition monitoring (OCM) and structural health monitoring (SHM) through acquiring measurements of temperature, strain, local stresses, pressure, structural vibrations, among other possibly indirectly interpreted measurands such as the propellants density and viscosity. Diagnosis and prognosis of the structure and the system is enabled through the structural damage estimation that these embedded sensors may accurately provide after dedicated data analysis and interpretation. Gauging estimation can be provided through the currently discussed architecture, but a dedicated architecture shall be integrated in the propellant management devices of the tank in case of prolonges space operations of the propulsion system. A smart propellant tank would employ integrated heaters to control the propellant temperature and provide active and localized thermal management and hence contributing to the propellant management activities.

In this paper, the Fiber Bragg Grating (FBG) type of optical fiber sensors (OFS) will be addressed as an embedded sensor in carbon fiber composite propellant tanks of spacecraft and launch vehicle upper-stages. The FBG sensor network would take part in the operations and condition monitoring (OCM) and the structural health monitoring (SHM) of the tank as a part of the propulsion system and the structural system of the spacecraft measuring mainly the temperature and the local strain of the structure, and consequently deriving measureands such as the structural local stresses and pressure loading besides the structural vibrations.

The challenges in employing such enabling-technology, namely the embedded optical fiber sensors, lies in the several aspects starting from the manufacturing

process of the host structure and the embeding technique including the ingress and egress of the optical fiber, and then the data processing and measurands interpretation. Thus, an optical fiber placement technique is introduced, namely the maximum principal strain optical fiber sensor placement method. In addition, an opto-mechanical model is derived to interpret strain transfer mechanism from the host structure to the sensor and relate the measured local strain to the local stresses in the embedding structure. The opto-mechanical mathematical model is derived from previous activities in literature [4] [5] [6] and adapted following the theorized optical fiber sensor placement technique.

Data acquisition units, namely the optical interrogators are separate units from the structure that gather and interpret the data from the embedded optical fibers. Due to the wide variety of commercial interrogators of FBG sensors besides those under development, the topic will not be addresses in this paper; however, commercial interrogators are available with a wide variety of performances and specifications and were demonstrated in space applications during the last decade or more [7] [8] [9].

2. Optical Fiber Sensors for Spacecraft OCM & SHM

A Fiber Bragg Grating (FBG) sensor is one of the most versatile and highly reliable optical fiber sensors used in sensor networks in diverse applications. Other types of optical fiber sensors relying on the light backscattering phenomena are becoming of great interest in aerospace applications as well, still the simplicity of FBG interrogation and its dynamic measurement capabilities besides the ability to employ in different sensor-network architectures makes it a first choice for space systems designers. The FBG is inscribed in the optical fiber core inducing a periodic modulation of the effective refractive index (n_{eff}). The FBG sensor is able to measure static and dynamic strain and temperature changes as main measurands. The reflected spectrum of light within the inscribed optical fiber allows for measuring the Bragg wavelength shift and the measurands are interpreted after a demodulation and signal processing of the calibrated acquired data. FBG sensor networks integration has become a research hotspot for quasi-distributed sensing [10]. Silica-based FBG sensors are capable of operating at range of temperature between -60 and 80 °C with acrylate coating without suitable packaging with metallic or polymeric material having higher thermal expansion coefficient [11] [12] [13]. FBG sensor sensitivity varies depending on the sensor material, packaging, and fabrication besides the interrogation method as well as the bonding or embedding technique, however, a typical strain sensitivity for silica fibres at 1550 nm is approximately 1

pm/µε while the temperature sensitivity is approximately 11 pm/°C.

Quasi-Distributed Optical Fiber Sensing

Quasi-Distributed Optical Fiber Sensing (Q-DOFS) based on FBG is fulfilled by multiplexing several inscribed sensors in a single optical fiber and several fibres are then connected to form network of optical fiber FBG inscribed sensors. Wavelength Division Multiplexing (WDM) technique is used to interrogate multiple FBGs in a single fiber by assigning a unique wavelength signature to each FBG. To counter the limited capability of multiplexing by WDM which is typically less than 100 nm available bandwidth [10] [14] Time Division Multiplexing (TDM) can be used conjunctly. WDM however possesses higher accuracy than TDM with the ability to measure temperature and strain with resolution of 0.1 °C and 1 µε with WDM instead of 1 °C and 10 µε with TDM. Several architectures and network schemes can be employed to fulfil the monitoring system requirements, referring to Figure 1.
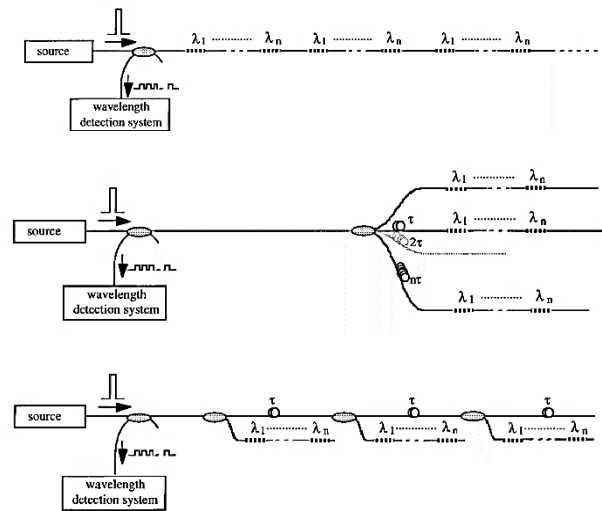

Figure 1. TDM and WDM multiplexing for network architectures of FBG sensors arrays. (a) Serial sensors network; (b) Parallel sensors network; (c) Branched sensors network. Courtesy of [49].

Distributed Optical Fiber Sensing

Distributed Optical Fiber Sensing (DOFS) employs the whole optical fiber as the sensing element, in contrast with the FBG-based sensing where inscribed points on the full-length optical fiber are the sensing elements as in the case of the Q-DOFS. In such case, the fiber detects changes in the scattered light wave characteristics along the fiber length due to local variation of physical parameters such as temperature and strain [15]. There are several methods of light scattering employed in fiber

optic sensing, Rayleigh scattering elastic physical phenomenon is one of the three major mechanisms used for DOFS. Rayleigh scattering is caused by non-propagating density fluctuations and is a linear process where the scattered light power is directly proportional to the input power. Rayleigh scattering is the easily distinguished central peak at the frequency of the typical spectrum backscattering light in an optical fiber surrounded by the stokes and anti-stokes spectral components of Brillouin and Raman scattering. Rayleigh scattering happens at the same frequency of the pump signal while Raman and Brillouin scattering, being inelastic, are characterized by the stokes and anti-stokes components. Rayleigh scattering can be detected in both frequency and time domains, namely the Optical Frequency Domain Reflectometry (OFDR) and Optical Time Domain Reflectometry (OTDR) [16].

OFDR has received special attention in research and development activities employing distributes sensing because of its relatively high resolution coupled with the high dynamic range [17]. The system relies on a tuneable laser that generates light to be split by a coupler between a measurement path and a reference path of an interferometer or referred to as probe and reference signals in other literature. The use of a tuneable laser source allows for high resolution in terms of millimetres over a fiber length of almost 100 m. The back reflection of the light from the fiber optic line that acts as the sensor element is recombined with the reference path. A Fourier Transform (FT) of the detected signal provides the phase and amplitude as a function of time along the optical fiber. The processed data obtained by the FT is partitioned around a specific location along the optical fiber, that is the sensing location, and the length of this partition or window acts as the actual spatial resolution attained in the physical parameter measurement, that is the strain. The back scattered spectrum is correlated with the reference spectrum and the spectral shift herein is converted to strain or temperature or both using a calibration factor. The process along the whole optical fiber can be iterated to obtain a distributed measurement of strain [15] [18] [19]. Commercial OFDR system can currently ensure a strain range of ±10,000 με within temperature range of -268 to +900 °C. Di Sante (2015) discussed in [15] that the available combinations of sensing length and acquisition rate can range from 2 m to 20 m at rates of 250 Hz and 50 Hz with accuracy of ±5 με and ±10 με, respectively, at a 5.12 mm gauge length. The lowest gauge length achievable, as recorded by the same author, is 1.28 mm with an accuracy of ±20 με where the acquisition rate decreases to ≈ 23 Hz and a sensing length of 10 m. On the other hand, for the quasi-static acquisition ≈ 2 Hz, the maximum sensing length can reach 50 m with a spatial resolution of 1 mm and accuracy of ±2 με.

Interrogation technologies

Both Q-DOFS based on FBG sensors and DOFS based on Rayleigh backscattering and OFDR have possessed great interest in aerospace and space applications and already possess a decades long heritage in terrestrial applications. Several aspects distinguish Q-DOFS based on FBGs with respect to other technologies, namely the fabrication and handling simplicity and cost efficiency particularly in the matter of data acquisition and interrogation. Interrogators of FBGs with different methods, span a wide range of frequencies and sensing rates to suit all applications of OCM and SHM. The interrogator size and mass and power consumption have proven successful operation in space missions of small-satellites even after countering a single event effect and destructive doses of radiation [8]. Further miniaturization activities for Q-DOFS FBG sensor interrogators have been carried out and realized products are expected in the very near future due to the advancements in Silicon on Insulator (SoI) and Photonic Integrated Circuits (PIC) enabling technologies for the fabrication of performant miniaturized FBG optical interrogators [20] [21]. As per the current time of publication of this paper, the OFDR-based distributed optical fiber sensing interrogation is still not realized in photonic integrated circuits PIC-based miniaturized interrogators although many research activities are being carried out towards this aim [22].

3. Opto-Mechanical Strain-Stress Transfer Model

A mechanical transfer model for the measurands of the optical sensor is required to be able to interpret meaningful and correct values of these measurands. Embedding or surface-bonding of optical fiber sensors to structures and systems' components is practiced on different types of materials. For the interest of aerospace and space applications, the structures of spacecraft or vehicle components are made of metallic materials and composite materials [23] [24] [15]. The main challenge herein is to analyse and interpret reliably the strain transfer from the structure to the optical fiber sensor while handling the temperature cross-sensitivity of the optical fiber in order to provide a correct and accurate value of the localized mechanical strain and the temperature, thus being able to derive subsequent measurands such as stresses and loading effects, among others.

Li, H.H. *et al.* (2009) [4] where able to sculpt one of the important articles in literature dealing with the modelling and analysis of strain/stress transfer for embedded FBGs in different host materials. Their article [4] has introduced an improved strain transfer model with respect to previous literature to evaluate the strain transfer efficiency from the host material to the fiber sensor core employing the theory of shear-lag. They were able to explore the strain transfer on a multilayered

concentric model counting for the fiber core, the interlayer, and the host material of the structure.

Sun et al. (2015) [25] derived a strain formula using both elastic analysis and the shear-lag method while considering several assumptions accounting for temperature variations and the non-axial stresses. The validated analytical results through the bare optical fiber behaviour simulation using finite element analysis have enabled to identify the parameters influencing the strain transfer from the host material of the structure embedding the FBG sensors as well as the temperature variation and cross-sensitivity impact; noting that one of the most appealing consideration Sun et al. have made, from our point-of-view, was the sensor alignment angle on the measurement accuracy.

The sensor alignment angle in the embedding process is one of the major considerations driving our mathematical opto-mechanical model presented in this paper. Nanni et al. (1991) [26] as cited in [24], has demonstrated that the embedding direction with respect to the applied load influences the performance of the sensors.

On another note, Gasior et al. (2021) [27], working on the development of non-destructive testing methods utilizing optical methods including optical fiber sensing based on FBGs for type 4 high pressure composite vessels, have presented interesting graphical results presenting deformations recorded by FBG sensors with respect to the FEA model simulations and one of the other optical methods used. These graphical results of the deformation recorded by the FBG sensors were based on the FBG surface-mounting scheme they used to assess the strain field in the cylindrical section of the pressure vessel and one of the dome sections. What grabbed our attention was the recorded relative error results for the FBG mounting direction in the longitudinal and circumferential directions where in the cylindrical part of the pressure vessel's liner, the biggest relative error was visible on the longitudinal direction while the circumferential direction of the same cylinder part the recorded maximum relative error did not exceed 5%.

These latter results by Gasior et al. (besides the former indications by Nanni et al.) about the influence of the FBG sensors performance driven by the embedding direction have affirmed our preliminary theory of *"embedding optical fiber sensors in the maximum principal strain direction"* that is dependent on the type and shape of the structure and the type of loading but can easily be indicated and predicted by finite element method simulations.

3.1. Maximum Principal Strain Direction FBG Placement and Optical Fiber Embedding Method.

Referring to the previous literature analysis considering the alignment angle of the optical fiber sensors either in structural host-material embedding or in surface-mounting (referred to as well by surface-bonding) it is perceived that the alignment direction impacts the sensor measurement performance and measurands accuracy and the relative error.

From a systems' design optimization view, by considering the number of sensor elements within an array and their effect on the monitoring system and signal processing complexity (thus the indirect effect on the cost and size of the interrogation unit), it is proposed that placing the FBG sensor element parallel to the maximum principal strain direction would be sufficient to detect the strain value. This would allow to analyse the subsequent local stress value, thus enabling the interpretation of foundation measurand data necessary for the structural health monitoring (SHM), structural and system operation diagnosis and prognosis, as well as operations and condition monitoring (OCM).

It is proposed that: *"an optical fiber array of FBGs or a backscattering-based optical fiber sensor can be embedded or surface-mounted placing the sensing element in consideration in a direction parallel to the direction of the relevant local maximum principal strain on the structure in hand considering the loading conditions and the boundary conditions during system operation."* – the maximum principal strain direction is believed to be reliably and easily predicted using the design simulations employing finite element methods and further validated through experimental tests.

3.2. An Opto-Mechanical Model for OFS Embedding

Further, in order to process and interpret the measurands data acquired by the monitoring system after the sensors' placement following the proposed method that considers the orientation of the sensor element (i.e., alignment direction of the optical fiber sensor following the maximum principal strain placement proposal) it is necessary to adapt a suitable mathematical model to relate the strain transfer rate, from the structure to the optical sensor, to the localized stress knowing the material properties of the structural host-material (or the adhesive material's mechanical characteristics in case of surface-bonding). – Accordingly, a suitable simplified *"Opto-mechanical model for local strain-stress identification of Optical Fiber Sensors' measurements embedded in Carbon Composite Structures"* is derived after adapting relevant considerations previously addressed in the discussed literature.

Assumptions

a. Embedding of optical fiber FBG sensors within the carbon fiber tape-wound layers of a pressure vessel, ensuring the sensing direction parallel to the layer averaged maximum principal strain placing the sensing element between unidirectional prepreg patches as the layers of direct contact ensuring the

parallel alignment between the sensing direction and the fiber direction of the patches.

b. Assuming no relative slip, the bonding conditions between the fiber core and the interlayer and between the interlayer and matrix are ideal. – maintaining in consideration that the embedded fiber with polyimide coating bonds well with the parallel/aligned carbon fiber after curing; moreover, the sensing fiber is too small to degrade the mechanical properties of the laminate.

c. The strain transfer from the matrix to the glass core of the optic fiber takes place via the shear strain of the interlayer. The interlayer and the glass core of the optic fiber are not directly subjected to external load. The Birefringent effect resulting from the lateral and radial strain on the FBG is considered to be negligible, thus only axial displacements can occur in the optical fiber and the interlayer with no radial deformation. – in reality there is a wavelength shift on the reflected Bragg peak when the sensor is subjected to lateral or radial stresses, however the wavelength variation is very small compared to wavelength variation induced by axial displacement and by temperature changes felt by the sensor.

d. All elements including the optical fiber, the interlayer, and the host-structure material are considered to be linearly elastic before and after deformation. – this is realistic only if the composite structure operates below yield conditions and no other structural failure or leaks appear on the mandrel.

e. It is reasonable to ignore effects of small temperature fluctuations on the strain change due to the comparably low-thermal expansion coefficient (0.73e-6 /°C) of the carbon fiber laminates.

The strain transfer model

Strain is caused by mechanical and thermal stresses; therefore, the total strain can be represented as:

$$\Delta\varepsilon^{tot} = \Delta\varepsilon^{mech} + \Delta\varepsilon^{th}$$

Recurring to the single-suffix notation for the strain components of the second-rank symmetric tensor, we can write:

$$\begin{Bmatrix}\varepsilon_1\\\varepsilon_2\\\varepsilon_3\\\varepsilon_4\\\varepsilon_5\\\varepsilon_6\end{Bmatrix} = \begin{Bmatrix}\varepsilon_1^{mech}\\\varepsilon_2^{mech}\\\varepsilon_3^{mech}\\\varepsilon_4^{mech}\\\varepsilon_5^{mech}\\\varepsilon_6^{mech}\end{Bmatrix} + \begin{Bmatrix}\varepsilon_1^{th}\\\varepsilon_2^{th}\\\varepsilon_3^{th}\\0\\0\\0\end{Bmatrix}$$

Considering no shear due to thermal expansion.

Indices from 1 to 3 indicate normal strain, while indices from 4 to 6 represent shear strain. The thermal strain (ε^{th}) is related to the difference in thermal expansion coefficient between composite structure (subscript 'c') and optic fiber sensor (subscript 'f'):

$$\Delta\varepsilon_i^{th} = (\alpha_{i,c} - \alpha_{i,f})\Delta T\left(1 - \frac{E_f}{E_c + E_f}\right)$$

Referring to the right most term, the repartition coefficient, depending on the stiffness of the two components, the strain will be distributed accordingly, with lower significance on the stiffer component and more significance on the softer component. It is important to note that a more rigorous formulation would require considering the coefficients of the stiffness tensor not only the E that represents the elastic behaviour only in the principal direction; in other words, if the stress and strain are not aligned to the principal direction, it will be needed to introduce the complete elastic tensor of the material.

Regarding the mechanical components of the strain transfer model and referring to Li et al. (2009) [4] and Soh et al. (2012) [28] the model defines three elements: the sensor, the interlayer, and the host-material, as shown in Figure 2. The formulation related the external strain field to the strain field on the embedded sensor. With the assumption of the stress direction to be parallel to the sensor axis, the solution representing the strain in the fiber in relation to the strain in the matrix and to the characteristic length of the sensor deforming along the x-direction would be:

$$\varepsilon^{mech}(x, r_f) = \varepsilon^{mech}(x, r_m)\left(1 - \frac{\cosh(kx)}{\cosh(kL)}\right)$$

Where k is a shearing-stress transfer parameter depending on the fiber core Young's modulus and interlayer and host material shear modulus and the radius of the fiber core, interlayer, and host material. It is defined as:

$$k^2 = \frac{1}{\frac{1}{2}r_f^2 E_f\left\{\frac{1}{G_i}\ln\left(\frac{r_i}{r_f}\right) + \frac{1}{G_m}\left[\frac{r_m^2}{r_m^2 - r_i^2}\ln\left(\frac{r_m}{r_i}\right) - \frac{1}{2}\right]\right\}}$$

The strain-optic tensor

The components of the strain-optic tensor represent the photo-elastic coefficients of the optic sensor and are dependent on the materials the sensor is made of. Referring to Chen and Albert (2006) [5], the ratio of the effective refractive index change of the sensor's fiber core to the change in strain is represented as:

$$\frac{\delta n}{\delta \varepsilon} = \frac{1}{2} n^3 [p_{12} - v(p_{11} - p_{12})]$$

Where n is the refractive index while p_{11} and p_{12} are the referent components in the strain-optic tensor for the isotropic media. The strain-optic tensor of isotropic media is represented as:

Figure 2. Embedded optical fiber sensor model cross-section. Courtesy of [4].

$$p = \begin{bmatrix} p_{11} & p_{12} & p_{12} & 0 & 0 & 0 \\ p_{12} & p_{11} & p_{12} & 0 & 0 & 0 \\ p_{12} & p_{12} & p_{11} & 0 & 0 & 0 \\ 0 & 0 & 0 & 0.5*(p_{11}-p_{12}) & 0 & 0 \\ 0 & 0 & 0 & 0 & 0.5*(p_{11}-p_{12}) & 0 \\ 0 & 0 & 0 & 0 & 0 & 0.5*(p_{11}-p_{12}) \end{bmatrix}$$

as noted in Ghatak and Thyagarajan (2012) [29], where fore the fused silica, the photo-elastic coefficients are $p_{11} = +0.121$ and $p_{12} = +0.270$.

Simplified local stress formula

For the optical fiber sensing element, namely the FBG sensor, placed along direction 1, that is the longitudinal direction parallel to the stress direction or the maximum principal strain as proposed in the placement method, the stress component can be derived as follows:

$$\sigma_1 = \frac{E\left(\frac{\Delta\lambda}{\lambda} - C_T \Delta T\right)}{(1-v^2)\left\{1 + \frac{1}{2}n^2[p_{12} - v(p_{11}-p_{12})]\left(1 - \frac{\cosh(kx)}{\cosh(kL)}\right)\right\}} - \frac{(\alpha_{i,c} - \alpha_{i,f})\Delta T \left(1 - \frac{E_f}{E_c + E_f}\right)}{(1-v^2)}$$

The formula represents the local stress components sensed by one FBG sensor element. The σ_1 formula is function of both the change in strain $\Delta\varepsilon^{tot}$ and change is temperature and knowing the ΔT value at the local measuring point, the temperature dependence can be compensated.

The topic of discriminating the temperature dependence within the Bragg wavelength shift formula of the FBG is widely discussed in literature. The most preliminary method is to embed a loose FBG sensor at the site of interest that isolates the grating element from any mechanical deformation effects besides the sensor initial calibration, thus discriminating the temperature change value.
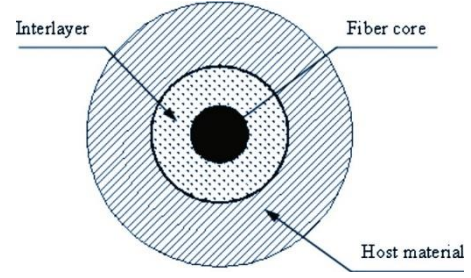
Key considerations

Several key considerations are taken when embedding optical fiber sensors in carbon composite structures and particularly in the discussed case of tape-wound pressure vessels.

a. Interlayer influences: material and geometry

In literature discussing the FBG embedding influencing parameters on the strain-stress transfer, the interlayer was thoroughly analyzed considering several points. The interlayer essentially can be a single layer in case of an embedded bare fiber where that interlayer represents the epoxy resin material filling between the glass fiber and the host structure's material. In the case of coated or optic fiber or a packaged optic fiber with, for example, polymeric or metallic material, it is essential to consider the strain transfer and the shear-lag between these multi-layers. Thus, the key aspects to be taken in consideration for the strain transfer analysis is:

- the interlayers number,
- the interlayer thickness,
- the shear-modulus of the inter layer and
- the influence of Poisson's ratio of each interlayer.

Li *et al.* (2009) test-validated most of these parameters in the referent study [4]. Monette *et al.* (1992) [30] concluded that the strain distribution in the fiber is expressed as a function of the Young's modulus ration of the fiber to the matrix. In addition, and after outlining the theory based on the shear-lag approach, it was noted that the shear strain in the matrix existed from the interphase to a point with a given distance inside the matrix. Following, Li and Grubb (1994) [31], as cited in Li *et al.* (2009), have used spectroscopic testing method to eventually obtain that in fact the shear-lag constant can be expressed as a function of the matrix shear modulus as

well as geometrically as a function of the *effective interfacial radius as they indicated by* r_e. This effective interfacial radius r_e is the radius for which the strain in the matrix equals the average matrix strain. Further their experimental measurements indicated that the r_e is on four times the fiber radius. Fig 3 shows the size scale of the optical fiber sensor diameter embedded in the epoxy resin host material of composite structures with different fiber orientations, [32] as cited in [15].
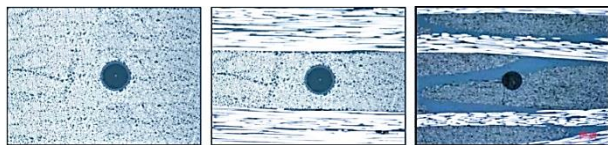
Figure 3. Embedded optical fiber sensor cross-section in different fiber composite orientation. Courtesy of [32] as cited in [15] under Creative Commons.

Another important material-based influence on the strain transfer is the shear modulus of the host structure material. The average strain transfer ratio is well-known to increase non-linearly with the increase of the shear-modulus of the host material. A thorough quantitative investigation is demonstrated in the study of Li et al. (2009).

b. Embedding environment and harnessing effect

After highlighting these influencing parameters on the strain transfer model, it is important to frame key considerations directly related to the application of this type of sensors in aerospace and space high-pressure composite vessels used as propellant tanks.

The high-pressure at the beginning of life storage and subsequently the pressure decay with the consumption of the propellant combined with operation-environment phenomena such as the outgassing should be carefully addressed and accounted for during the design of these advanced monitoring systems for space applications since a significant effect is expected on the embedding mechanical and material characteristics of the host structure.

Furthermore, the storage temperature gradients especially in extreme storage-temperature cases should be carefully addressed not only from the point-of-view of the optical fiber cross-sensitivity elimination but also from the mechanical and material characteristics impacted by the storage temperature and thus affecting locally and individually each of the embedded sensors.

Hence, an effect that should be locally considered for each sensor re-calibration after the embedding process as well as during the operations-process that counts mainly for the environmental and operational impacts on the mechanical and material embedding aspects influencing the strain rate transfer and the strain-stress model between the optical fiber sensor and the host-structure

material is the harnessing effect. The word harnessing is used here to describe how the sensor element is harnessed or spatially maintained in the embedding location as designed to be.

4. Smart Tank Prototype Preliminary Design

Propulsion systems of spacecraft and launcher's upper-stages (i.e., kick-stages) are currently eyeing a major transition towards carbon composite structures manufacturing technology to increase the system's performance through weight reduction when compared to metallic structures. The carbon pressures vessels with their types (type III and type IV) are widely commercially used in propulsion systems – type III being the tank with metallic liner and carbon composite fully overwrapped load-bearing structure, while type IV being the plastic (polymer-based) liner surrounded by a thicker layer of carbon fiber composite overwrapped load-bearing structure. The carbon composite propellant tanks are used in primary and auxiliary reaction and attitude control subsystems of the propulsion system, either in satellites or upper stages of launchers.

The preliminary design in the current study is intended for the proof-of-concept of a smart tank utilizing optical fiber sensors (i.e., FBG quasi-distributed sensors and distributed optical fiber sensors based on Rayleigh backscattering) and made of a carbon composite wound pressure vessel that is approximately 40L in volume and would be fabricated in two versions, one employing a metallic liner (e.g., Titanium or Aluminium based alloys) and another employing a polymer liner (e.g., PVC or PTFE). The target storage fluids are the EIL green monopropellants that are characterized by negligible vapor pressure; and pure nitrous oxide in gaseous and liquid storage phases as another green oxidizer propellant that is storable and transportable and possesses high density and low pressure when maintained at low temperature (i.e., typically stored under saturated conditions at 5.2 MPa and ambient temperature), besides its recreational uses.

Propellant Storage in Spacecraft

Typically, large propulsion systems of mid-to-high lift launchers rely on one or more cryogenic propellant, either a cryogenic oxidizer component besides a hydrocarbon (e.g., RP-1), or both cryogenic oxidizer and fuel components (e.g., LOX and LNG or LH, etc.) Smaller propulsion systems of small launchers upper-stages as well as satellites are gaining a trend in using green propellants such as hydrogen peroxide, energetic ionic liquids (EILs), and NOx-based propellants, either in monopropellant or bi-propellant configurations or in multi-mode propulsion architectures [33] [34] [35] [36]. Two classes of green propellants are considered for the

current study, namely the energetic ionic liquids (EILs) and the nitrous oxide NOx-based propellants.

EILs or the energetic ionic liquids are premixed oxidizer/fuel ionic propellant blends consisting of oxidizer salts dissolved in aqueous solutions referred to as ionic liquids that are mixed with ionic fuels or molecular fuels forming a premixed propellant widely referred to as monopropellants in literature [37] [36]. The propellant possesses high solubility and negligible vapor-pressure of its solution constituents, thus contributing to low toxicity hazards and high mixture stability at different temperature levels, that consequently makes exposure to open environments have almost no safety concerns [38].

Nitrous oxide in the compound form is used as an oxidizer in both hybrid and liquid bi-propellant engines. It takes part as well in the NOx-based monopropellants or as referred to by Nitrous Oxide Fuel Blends (NOFB) and can be used solely in the pure form as a monopropellant with much lower performance than the previous uses.

N_2O (liquid) storage density is approximately 0.745 g cm^{-3} at 20 °C and around 5.2 MPa vapor pressure [39]. The saturated vapor pressure of ~5.2 MPa, is high compared to EILs, but is still favourable when accounting for the self-pressurizing abilities of this propellant. The critical point stands at 36.4 °C and 7.24 MPa [40] and is in saturated liquid-vapor mixture in the temperature–pressure range of [−30, +28] °C and [1.31, 6.0] MPa.

European Fuel Blend (EUFB) [41] [42] is a type of the NOFB that consists of nitrous oxide and ethanol which has a saturated liquid density of 0.892 g cm^{-3} with a stoichiometric O/F ratio of 5.73 (~14.86% fuel). The critical point stands at 36.45 °C and 6.3 MPa and the vapor pressure is 2.6 MPa. Design pressure for EUFB storage is 7.0 MPa while operating temperature range is ≥ 42 °C and the storage range is set from − 40 to +75 °C [43]. The most compelling about N_2O for modern propulsion system design is that it can be used in the so called "multi-mode" propulsion system [44], where it can act as a propellant for cold-gas, monopropellant propulsion, and/or bipropellant systems using the same propellant tank.

To ensure self-pressurizing capability of the propellant, the propellant temperature needs to be controlled by a Thermal Control System (TCS) to maintain the required operating pressure and to account for any pressure drop due to temperature excursions during all the mission phases, which is one of the aspects a smart propellant tank is expected to provide besides the sensing capabilities.

Propellant selection and testing considerations

The propellant selection at the current stage of design is based on the storage conditions and thermodynamic characteristics which will allow for a relatively simpler handling and testing procedures when compared to cryogens. Cryogenic propellants were considered in several studies such as that by Liang et al. (2022) where liquid nitrogen was used. EIL propellants are simply liquid propellants with non-detonable nature and negligible vapor pressure, this will allow for testing the smart tank employing the thermal control system under varying temperatures to observe the response of the optical fiber sensors under different temperatures; moreover, the green EILs will give more flexibility in handling. – water can be used for thermal and pressure testing; however, it is intended to further assess these ionic salt propellants flow in the pipeline components and fluid management system during the test campaign. On another account, nitrous oxide being stored at saturation conditions will allow for observing the smart tank structural resistance and the embedded sensors responses to the local strains/stresses under higher storage pressures when applying the needed temperature increments through the thermal control system (TCS).

Tape-winding of pressure vessels

Pressure vessels composite filament winding and the prepreg tape-winding are used by automated robotic fiber wrapping systems to fabricate revolving body composite structures. Prepreg tape-winding is well considered as an effective method for producing aerospace components of launch vehicles and satellites. Launch vehicle and missile parts manufactured by this method include solid rocket motors and missile body structure as well as the nozzles [45] [46]. The tape winding of carbon composite roving can produce polar, helical, and hoop winding of unidirectional or woven prepreg carbon fiber roving of predefined bandwidth and made of variety of fiber material. A design software is initially used to design the layers by defining the winding parameters such as the frame position and direction, the winding angle, the friction factor, and the roving bandwidth beside the material definition of the carbon composite roving.

It is proven in literature that the fabrication parameters such as the heating temperature, the applied tape tension and roller pressure, as well as the winding speed have an altering effect on the mechanical properties of the wound composite structure under development [47] [48].

The composites tape winding technique was regarded and used in the design of the smart tank prototype since it is believed to facilitate the optical fiber integration and embedding throughout the fabrication process considering the optic fiber placement and the sensing element attaching and orienting. Another consideration is

the accessibility of industrial grade software that enables a time efficient iterative design and analysis procedures.

CADWIND – composites winding software

The software was used to design and simulate the tape wound pressure vessel. The integrated mandrel generator allowed for iteratively design and analyse the mandrel geometry besides the possibility to import mandrel external CAD designs in different formats. The software allows for modelling of the friction parameter that represents the friction between the fibre and the mandrel or the fiber and the below layer. The friction factor is crucial in the non-geodesic winding modelling that accounts against the filaments and layer slipping – the geodesic path is the shortest distance between two points on a curved surface (i.e., the dome part in our case). The non-geodesic winding accounting for the friction factor is typically beneficial in the design and fabrication optimization. CADWIND has the ability to export the design to most of the academic FEA software with high fidelity tape-wound layers geometric characteristics and relying on updating the winding thickness and diameter automatically and maintaining the winding angle and thus a more realistic fiber direction during the FEA simulations. Finally, the fabrication simulation using different production techniques is possible and provides detailed machine motion and dynamics analysis which facilitates consequent prototyping phases.

In order to be able to embed the optical fibre sensors within the composite structures, it is essential to decide optimally both the location and orientation of the sensing element (i.e., sensing point) of the optical fibre sensors. To sufficiently perform this task, the composite fibre laminates orientation in each ply-layer has to be carefully determined in the structural analysis process, so as the fields of stresses and strains analysing both magnitude and direction.

The conventional composites design in ANSYS ACP does not provide the luxury of simulating Tape Winding, as CADWIND do. Instead, ANSYS ACP can simulate plies and layups of composite sheets each with a predefined specific orientation, but not the more sophisticated interwinding bandwidth of roving of composite tape. From here, CADWIND was proposed along with ANSYS Structural Analysis to be able to access more realistic simulation data that more precisely describe locations of interest and orientation of stresses and strains in points of interest within the layers of composite tape-wound.

4.1. Tank design and FEA structural analysis

The first prototype is designed to employ a liner of PVC or PE polymer materials and only three tape-winding layers. The MEOP in the first prototype is 1.8 MPa and nominal testing pressure is between 1 – 1.2

MPa. The simple design of the first prototype is intended to give experimental validation of the FEA results and to provide understanding of the layer-to-layer interaction while embedding the optical fiber sensors in designated locations and orientation. The interaction between the layers and the packaging UD patches is expected to be better observed rather than the case of higher MEOP design with a greater number of tape-wound plies (e.g., prototype two employs nine layers.)

Table 1 lists the geometric properties of the mandrel noting that the layer thickness is added recursively, and the external dimensions are exported automatically to ANSYS for the FEA structural analysis. – the thickness per roving ranges from 0.19 to 0.2 mm; the complete tape-wound layer thickness is calculated by CADWIND and is listed in Table 4. The overlaps of tape roving create thicker contours at the edges of the layers, as shown in the thickness distribution figures below.

Table 1. Mandrel geometric properties

Parameter	Value
Cylinder diameter	432 mm
Cylinder length	154 mm
Ellipsoid height	108 mm
Polar boss diameter	50 mm

Table 2. Winding material parameters

Parameter	Value
TEX value	1650 (g/km)
Fiber density	1.8 (g/cc)
Fiber vol. fraction	60%
Friction factor	0.12
Bandwidth single roving	8 (mm)
Bandwidth total	16 (mm)

Table 3. Tape-winding layers properties

Layer no.	Winding angle (deg.)
Layer 01	5
Layer 02	15
Layer 03	65

Table 4. Wound layers thickness extremes.

Layer no.	Min Thickness	Max Thickness
Layer 01	0.385	32.465
Layer 02	0.396	32.465
Layer 03	0.575	12.508

In the following figures (Figure 4 – 9) the CAD designs of the tape-wound three layers of prototype-one are shown in yellow and the blue-red coloured figures displaying the thickness distribution of the winding.
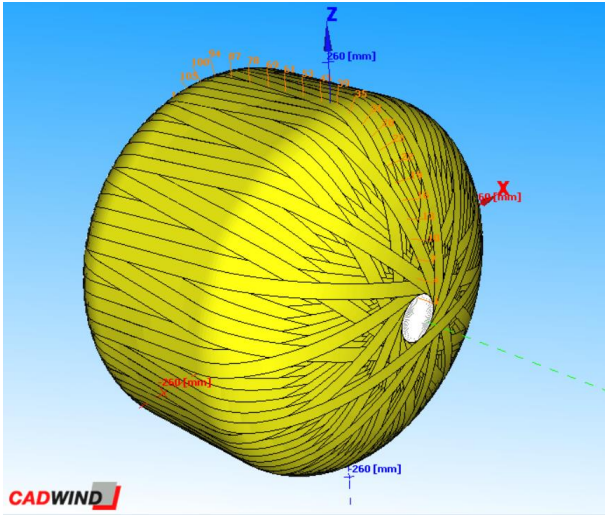
Figure 4. Layer 01 tape-winding at winding angle 5 deg.
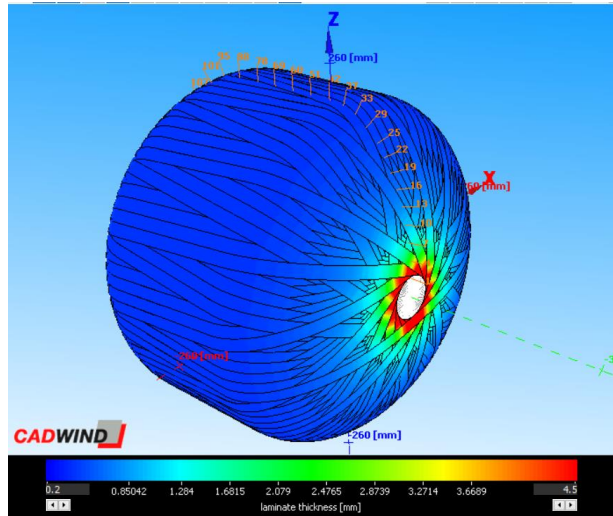

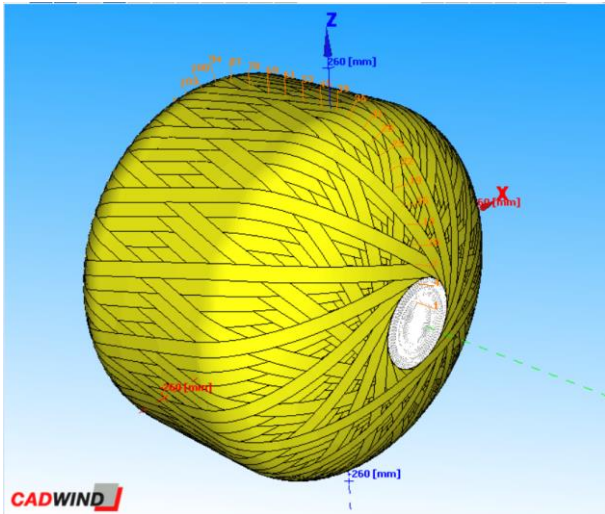Figure 7. Layer 01 laminate thickness distribution.

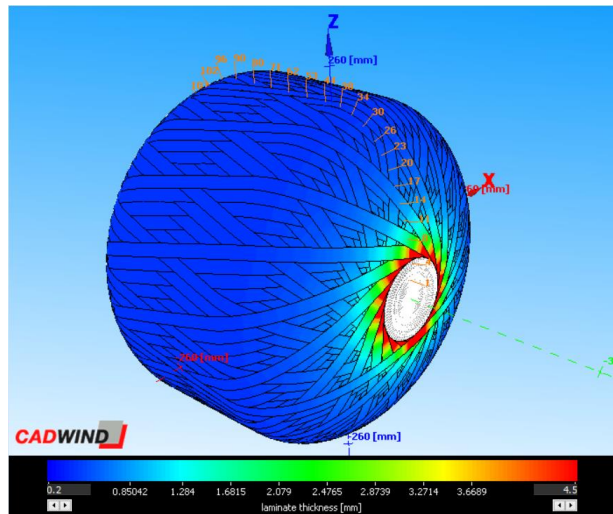Figure 5. Layer 02 tape-winding at winding angle 15 deg.

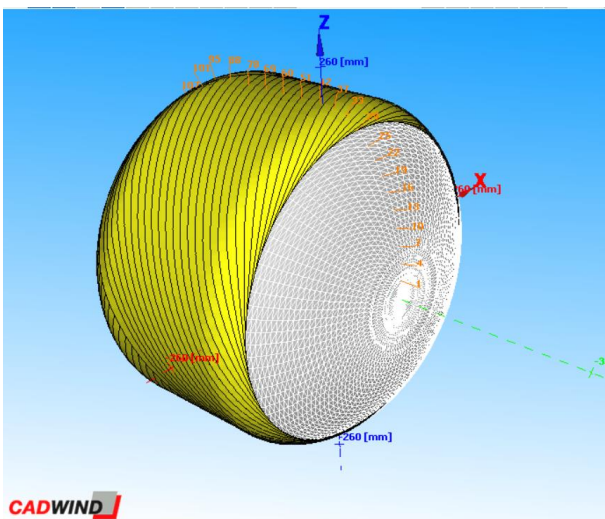Figure 8. Layer 02 laminate thickness distribution.

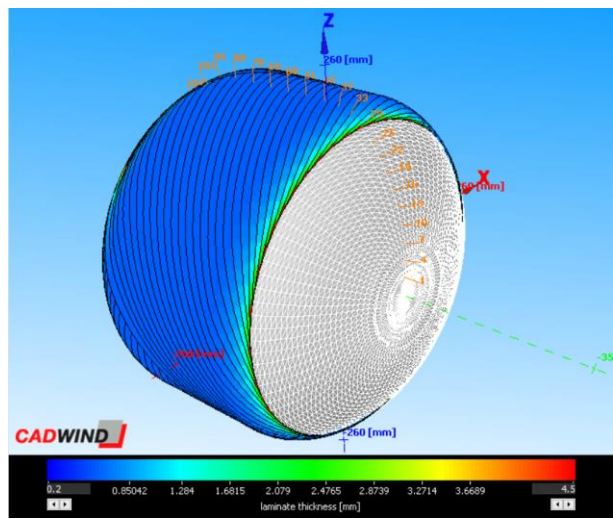Figure 6. Layer 03 tape-winding at winding angle 65 deg.

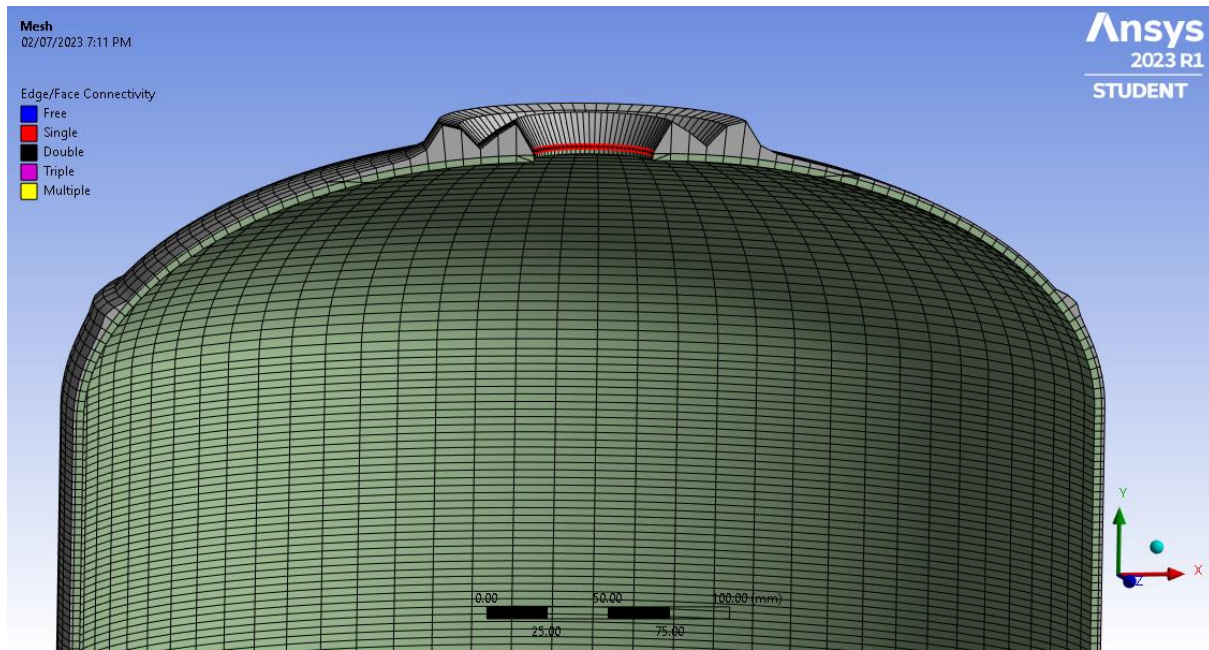Figure 9. Layer 03 laminate thickness distribution.

Figure 10. ANSYS imported design of three tape-wound layers and the liner/mandrel.
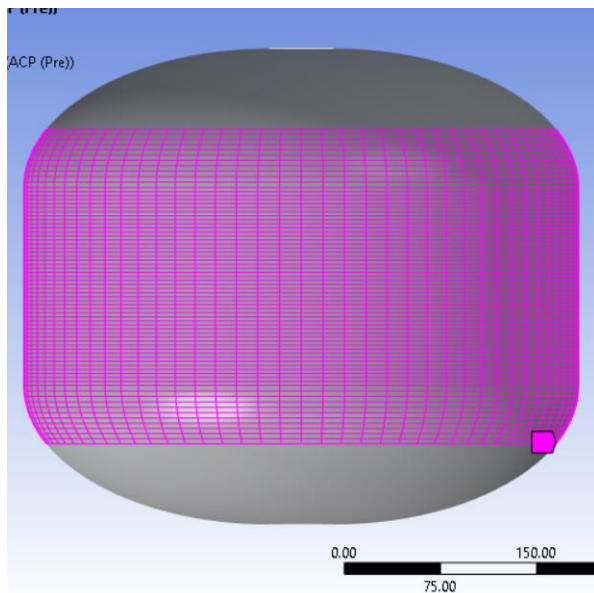

Figure 11. Layer 03 mesh.

ANSYS structural analysis is performed after the per-ply definition of the imported layers from CADWIND in Ansys Composite PrepPost (ACP). The file format used in this simulation was the "HDF5 Composite Data + Mandrel Model ANSYS CDB." Layer 03 mesh and fiber orientation angles is shown in Figure 11 and 12 as an illustrating example.
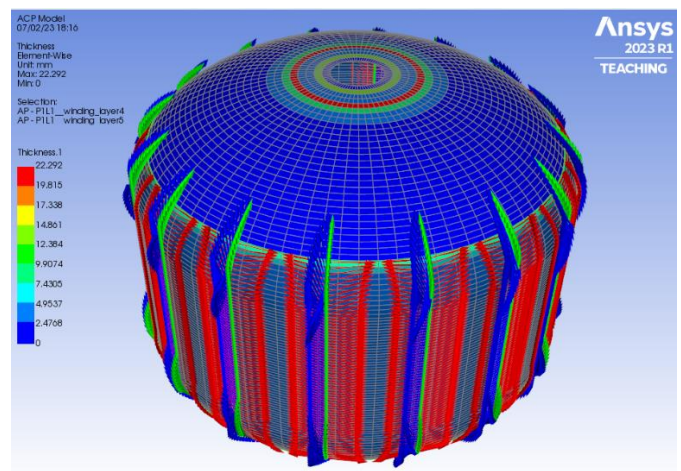
Figure 12. Layer 03 ACP Model showing fiber directions and in red and normal-to-fiber direction in blue.

The vector principal elastic strain solution is applied for each layer to identify and determine the orientation of the maximum principal strain vector – as shown in Figures 13 – 17. Further, the total deformation solution is shown in Figure 18 noting a maximum deformation value of 0.2 mm. Figure 19 displays the equivalent elastic strain solution for Layer 03, taken as an example, to have a maximum value of 0.657 mε.
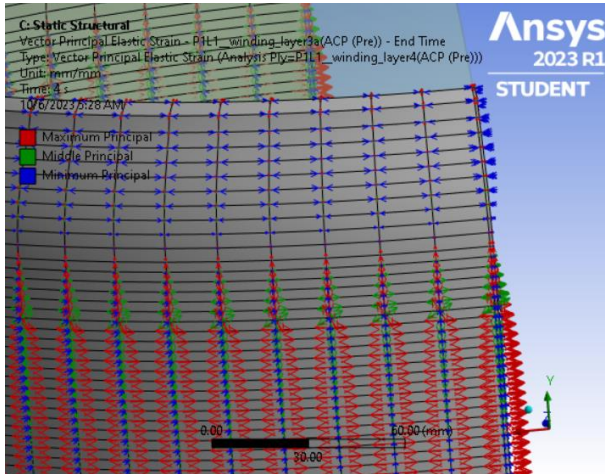
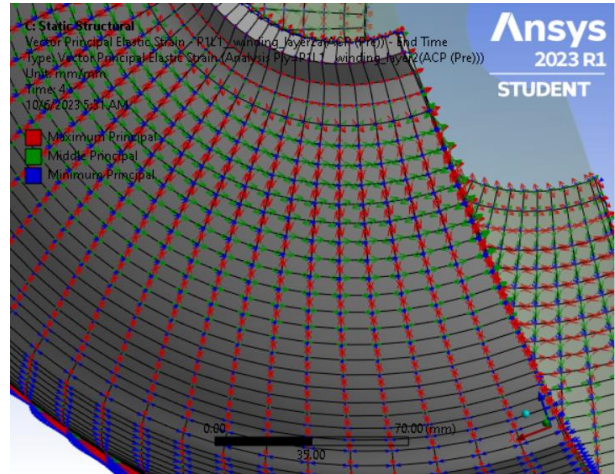Figure 13. Vector principal elastic strain solution – Layer 03.

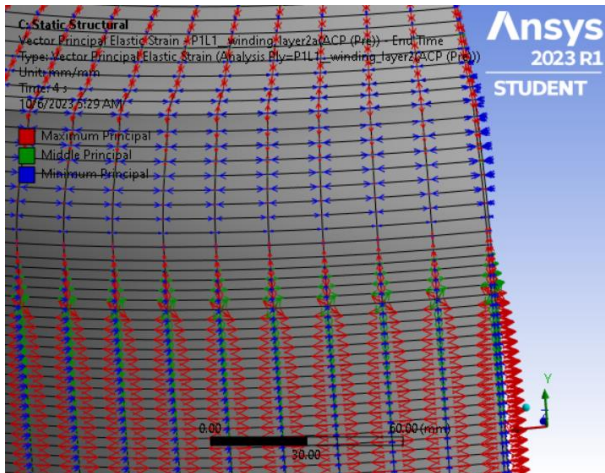Figure 14. Vector principal elastic strain solution – Layer 02.

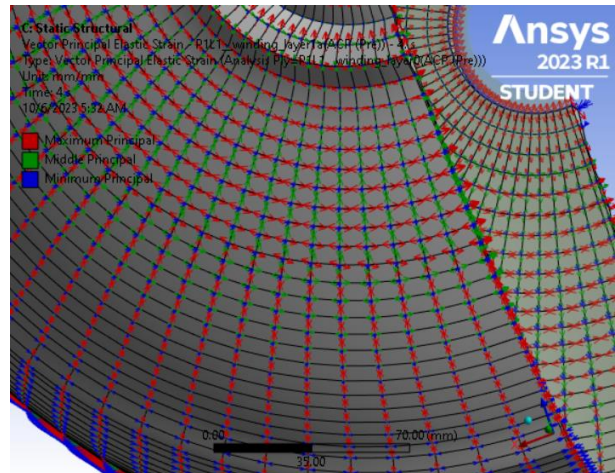Figure 15. Vector principal elastic strain solution – Layer 01.

Figure 16. Vector principal elastic strain solution – Layer 02.
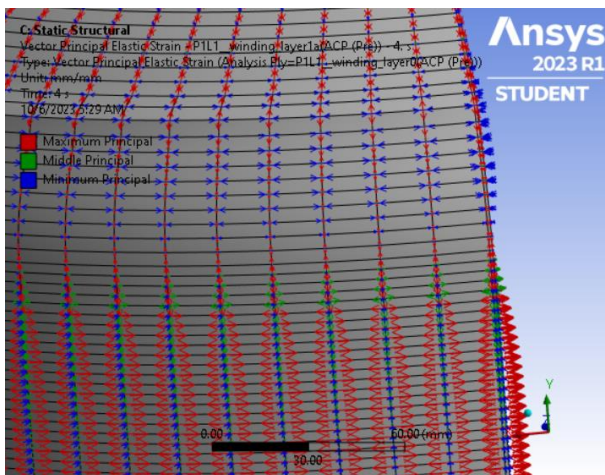

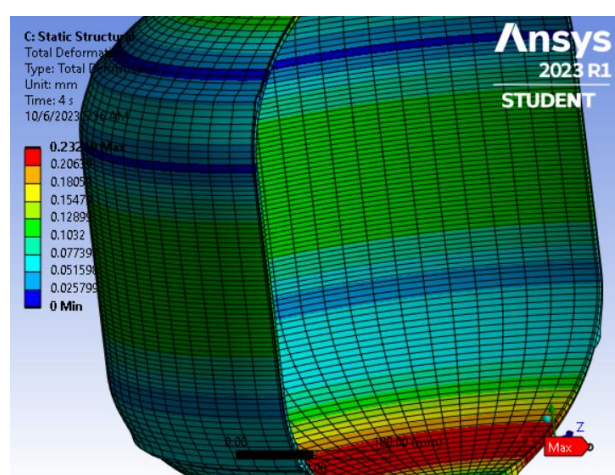Figure 17. Vector principal elastic strain solution – Layer 01.

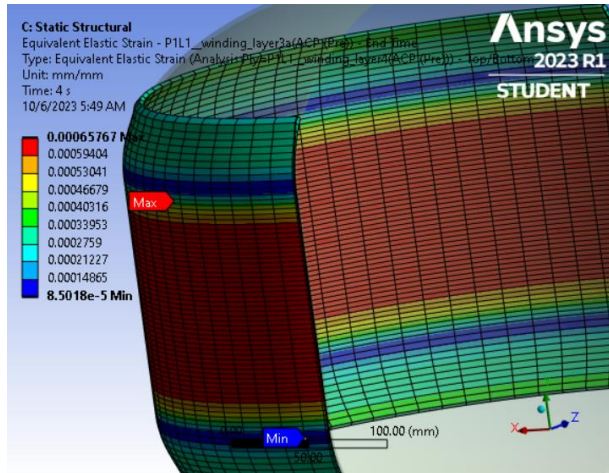Figure 18. Total deformation solution; maximum value of 0.232 mm.

Figure 19. Equivalent elastic strain solution for Layer 03 showing a max value of 0.6576 mε.

5. Conclusion

The preliminary structural analysis procedure of the carbon-composite tape-wound pressure vessel (i.e., in scope of a Smart Propellant Tank design) with a liner of either polymeric material, as in the case of prototype-one design or a liner of metallic material as in the case of prototype-two, shows that the data exported can assist in the optical fiber sensor embedding by identifying the points of interest. The points of interest are those with higher total deformation value and are the point near critical parts of the vessel where failure usually occurs.

The mapping of the elastic strain vector is predicted by the simulation to help in the identification of the correct orientation of the optical fiber sensor and the proper placement of the sensing element along the maximum principal strain direction, as theorized in section 3, following the statement *"embedding optical fiber sensors in the maximum principal strain direction"*; –According to the classic maximum principal strain theory, yielding will occur when the maximum value of principal strain will exceed the strain at the tensile yield point, which gives insight about the direction of placement of the sensor element if only the critical dimension assessment is sought.

In this paper, a mathematical model to interrelate the strain to stress value through the material elastic properties, i.e., the compliance matrix or the stiffness matrix of the material. This opto-mechanical model proposed is based on various strain transfer models discussed in literature that incorporates elastic and shear-lag analysis theories. The opto-mechanical model proposed in this paper highlights the local stress value in the maximum principal direction, where further physical properties and failure prediction can be derived from this value.

References

[1]   A. E. Nosseir, A. Cervone, A. Pasini, S. Igarashi and Y. Matsuura, "Additively Manufactured Green Propellant Tanks: Volume Efficient Designs and Materials Chemical Compatibility," *International Journal of Energetic Materials and Chemical Propulsion,* vol. 22, no. 6, p. 1–16, 2023.

[2]   European Space Agency, "ESA contracts ArianeGroup to press ahead with full-scale demonstrator of carbon fibre "black stage" to boost launch performance," 3 November 2022. [Online]. Available: https://www.esa.int/Enabling_Support/Space_Transportation/Future_space_transportation/ESA_contracts_ArianeGroup_to_press_ahead_with_full-scale_demonstrator_of_carbon_fibre_black_stage_to_boost_launch_performance. [Accessed 15 July 2023].

[3]   European Space Agency, "Tests prove carbon-fibre fuel tank for Phoebus upper stage," 20 January 2021. [Online]. Available: https://www.esa.int/Enabling_Support/Space_Transportation/Future_space_transportation/Tests_prove_carbon-fibre_fuel_tank_for_Phoebus_upper_stage. [Accessed 15 July 2023].

[4]   H.-N. Li, G.-D. Zhou, L. Ren and D.-S. Li, "Strain Transfer Coefficient Analyses for Embedded Fiber Bragg Grating Sensors in Different Host Materials," *Journal of Engineering Mechanics,* vol. 135, no. 12, pp. 1343-1353, 2009.

[5]   C. Chen and J. Albert, "Strain-optic coefficients of individual cladding modes of singlemode fibre: theory and experiment," *Electronics Letters,* vol. 42, no. 18, p. 1027 – 1028, 2006.

[6]   F. Ansari and Y. Libo, "Mechanics of Bond and Interface Shear Transfer in Optical Fiber Sensors," *Journal of Engineering Mechanics,* vol. 124, no. 4, pp. 385-394, 1998.

[7]   I. McKenzie, S. Ibrahim, E. Haddad, S. Abad, A. Hurni and L. K. Cheng, "Fiber Optic Sensing in Spacecraft Engineering: An Historical Perspective From the European Space Agency," *Front. Phys.,* vol. 9:719441, 2021.

[8]   E. Haddad, R. V. Kruzelecky, M. Mena and K. Tagziria, "Optical Fiber Sensors System on Proba-2 After 7 Years," in *Proc. of SPIE Vol. 10562, 105625S International Conference on Space Optics — ICSO 2016*, Biarritz, France, International Conference on Space Optics — ICSO 2016.

[9]   R. V. Kruzelecky, J. Zou, E. H. Najeeb Mohammed and e. al., "Fiber-optic sensor demonstrator (FSD) for the monitoring of spacecraft subsystems on ESA'S PROBA-2," in *International Conference on Space Optics (ICSO 2006)*, Noordwijk, Netherlands, 2006.

[10]   C. LI, J. TANG, C. CHENG, L. CAI and M. YANG, "FBG Arrays for Quasi-Distributed Sensing: A Review," *Photonics Sensors,* vol. 11, no. 1, pp. 91-108, 2021.

[11]   C. Broadway, R. Min, A. G. Leal-Junior, C. Marques and C. Caucheteur, "Toward Commercial Polymer Fiber Bragg Grating Sensors: Review and Applications," *Journal of Lightwave Technology,* vol. 1, pp. 2605-2615, 2019.

[12]   v.-L. Bundalo, K. Nielsen, G. Woyessa and O. Bang, "Long-term strain response of polymer optical fiber FBG sensors," *Optical Materials Express,* vol. 7, pp. 967-976, 2017.

[13]   J. K. Sahota, N. Gupta and D. Dhawan, "Fiber Bragg grating sensors for monitoring of physical parameters: a comprehensive review," *Optical Engineering,* vol. 59, no. 6, p. 60901, 2020.

[14]   Y. M. Wang, J. M. Gong, D. Y. Wang, B. Dong, W. Bi and A. Wang, "A Quasi-Distributed Sensing Network with Time-Division-Multiplexed Fiber Bragg Gratings," *IEEE Photonics Technology Letters,* vol. 23, no. 2, pp. 70-72, 2011.

[15]   R. Di Sante, "Fibre Optic Sensors for Structural Health Monitoring of Aircraft Composite Structures: Recent Advances and Applications," *Sensors,* vol. 15, pp. 18666-18713, 2015.

[16]   M. Froggatt and J. Moore, "High-spatial-resolution distributed strain measurment in optical fiber with Rayleigh scatter.," *Appl. Opt.,* vol. 37, pp. 3284-3286, 1998.

[17]   P. Lu, N. Lalam, M. Badar, B. Liu, B. T. Chorpening, M. P. Buric and P. R. Ohodnicki, "Distributed optical fiber sensing: Review and perspective," *Applied Physics Reviews,* vol. 6, no. 041302, 2019.

[18]   B. J. Soller, M. E. Froggatt, D. K. Gifford, M. S. Wolfe, M. H. Yu and P. F. Wysocki, "Measurement of Localized Heating in Fiber Optic Components with Millimeter Spatial Resolution," in *Optical Fiber Communication Conference, 2006 and the 2006 National Fiber Optic Engineers Conference. OFC 2006*, CA, USA, 2006.

[19]   B. J. Soller, D. K. Gifford, M. S. Wolfe and M. E. Froggatt, "High resolution optical frequency domain reflectometry for characterization of components and assemblies," *Optics Express,* vol. 13, no. 2, pp. 666-674, 2005.

[20]   Y. E. Marin, T. Nannipieri, C. J. Oton and F. D. Pasquale, "Current Status and Future Trends of Photonic-Integrated FBG Interrogators," *JOURNAL OF LIGHTWAVE TECHNOLOGY,* vol. 36, no. 4, 2018.

[21]   J. Elaskar, F. Bontempi, P. Velha, R. M. A. Ayaz, L. Tozzetti, S. Faralli, F. D. Pasquale and C. J. Oton, "Ultracompact Microinterferometer-Based Fiber Bragg Grating Interrogator on a Silicon Chip," *Journal of Lighwave Technology,* vol. 41, no. 13, pp. 4397-4404, 2023.

[22]   P. Pintus, J. Guo, M. A. Tran, W. Jin, J. Liang, J. Peters, C. Xiang, O. J. O. III and J. E. Bowers, "Demonstration of Large Mode-Hop-Free Tuning in Narrow-Linewidth Heterogeneous Integrated Laser," *Journal of Lightwave Technology,* 2023.

[23]   P. Ferreira, M. Machado, M. Carvalho and C. Vidal, "Embedded Sensors for Structural Health Monitoring: Methodologies and Applications Review," *Sensors,* vol. 22, p. 8320, 2022.

[24]   F. Falcetelli, L. Rossi, R. Di Sante and G. Bolognini, "Strain Transfer in Surface-Bonded Optical Fiber Sensors. Sensors," *Sensors,* vol. 20, no. 11, p. 3100, 2020.

[25]   L. Sun, H. Hao, B. Zhang, X. Ren and J. Li, "Strain Transfer Analysis of Embedded Fiber Bragg Grating Strain Sensor," *Journal of Testing and Evaluation,* 2015.

[26]   A. Nanni, C. Yang, K. Pan, J. Wang and R. Michael, "Fiber-optic sensors for concrete strain/stress measurement," *ACI Mater. J.,* vol. 88, p. 257–264, 1991.

[27]   P. Gąsior, K. Wachtarczyk, A. Błachut, J. Kaleta, N. Yadav, M. Ozga and A. Baron, "Validation of Selected Optical Methods for Assessing Polyethylene (PE) Liners Used in High Pressure Vessels for Hydrogen Storage," *Applied Sciences,* vol. 11, no. 5667, 2021.

[28]   C.-K. Soh, Y. Yang and S. Bhalla, Smart Materials in Structural Health Monitoring, Control and Biomechanics, Springer, 2012.

[29]   A. K. Ghatak and K. Thyagarajan, "16 - The strain optic tensor," in *Optical Electronics*, Cambridge University Press, 2012, pp. 501-507.

[30]   L. Monette, M. P. Anderson, S. Ling and G. S. Grest, "Effect of modulus and cohesive energy on critical fibre length in fibre-reinforced composites," *Journal of Materials Sceince,* vol. 27, no. 16, p. 4393–4405, 1992.

[31]   Z. F. Li and T. Grubb, "Single-fiber polymer composites Part I: Interfacial shear strength and stress distribution in the pull-out test.," *Journal of Materials Science,* vol. 29, p. 189–202, 1994.

[32]   G. Luycks, E. Voet, N. Lammens and J. Degrieck, "Strain measurements of composite laminates with embedded fibre Bragg gratings: Criticism and opportunities for research," *Sensors,* vol. 11, p. 384–408, 2011.

[33]   A. Sarritzu, F. Lauck, L. Werling and A. Pasini, "Assessment of Propulsion System Architectures for Green Propellants-based Orbital Stages," in *73rd International Astronautical Congress (IAC)*, Paris, France, 2022.

[34]   A. Sarritzu, L. Blondel-Canepari, R. Gelain, P. Hendrick and A. Pasini, "Trade-off study of green technologies for upper stage applications," in *Space Propulsion Conference*, Estoril Portugal, 2022.

[35]   A. E. S. Nosseir, A. Pasini and A. Cervone, "A Survey of Energetic Ionic Liquid Green Monopropellants and Investigation of Feed and Pressurization Systems For Small Satellites High-Thrust Impulsive Propulsion," in *Space Propulsion Conference 2020+1*, Virtual Event, 17-19 March 2021.

[36]   A. E. S. Nosseir, A. Cervone and A. Pasini, "Review of State-of-the-Art Green Monopropellants: For Propulsion Systems Analysts and Designers," *Aerospace,* vol. 8, no. 1, p. 20, 2021.

[37]   Y. Batonneau and R. Brahmi, "Application of Ionic Liquids to Space Propulsion," in *Applications of Ionic Liquids in Science and Technology*, Poitiers, France, InTech, 2011, pp. 447-466.

[38]   R. K. Masse, M. Allen, E. Driscoll and R. A. Spores, "AF-M315E Propulsion System Advances & Improvements," in *52nd AIAA/SAE/ASEE Joint Propulsion Conference*, Salt Lake City, UT, 2016.

[39]   J. Wallbank, P. Sermon, A. Baker, L. Coutney and R. Sambrook, "Nitrous Oxide as a Green Monopropellant for Small Satellites," in *2nd International Conference on Green Propellants for Space Propulsion*, Sardinia, IT, 2004.

[40]   National Institute of Standards and Technology - NIST Chemistry WebBook SRD69, "Nitrous Oxide," 2018. [Online]. Available: https://webbook.nist.gov/cgi/cbook.cgi?ID=10024-97-2. [Accessed 26 04 2020].

[41]   A. Mayer and W. Wieling, "Green Propulsion Research at TNO the Netherlands," *Transactions of The Institute of Aviation,* vol. 4, no. 253, pp. 1-24, 2018.

[42]   A. Mayer, W. Wieling, A. Watts, M. Poucet, I. Waugh, J. Macfarlane and F. Valencia Bel, "European Fuel Blend Development for In-space propulsion," in *Space propulsion Conference*, Seville, Spain, 2018.

[43]   A. Mayer, I. Waugh and M. Poucet, "European Fuel Blend Development Final Report - TNO 2018 R10640," European Space Agency, 2018.

[44]   J. L. Rovey, C. T. Lyne, A. J. Mundahl, N. Rasmont, M. S. Glascock, M. J. Wainwright and S. P. Berg, "Review of multimode space propulsion," *Progress in Aerospace Sciences,* vol. 118, no. 100627, October 2020.

[45]   R. Henriquez and P. Mertiny, "3.21 Filament winding applications," in *Comprehensive Composite Materials II*, Amsterdam, Holland, Elsevier, 2018, p. 556–577.

[46]   Z. Han, S. Sun, W. Li, Y. Zhao and Z. Shao, "Experimental study of the effect of internal defects on stress waves during automated fiber placement," *Polymers ,* vol. 10, no. 413, 2018.

[47]   N. Nath, "Optimization of tape winding process parameters to enhance the performance of solid rocket nozzle throat back up liners using taguchi's robust design methodology," *J. Inst. Eng. Ser. C,* vol. 98, p. 479–484, 2017.

[48]   A. Zaami, M. Schäkel, I. Baran, T. Bor, H. Janssen and R. Akkerman, "Temperature variation during continuous laser-assisted adjacent hoop winding of type-iv pressure vessels: An experimental analysis," *J. Compos. Mater.,* vol. 54, p. 1717–1739, 2020.

[49]   A. D. Kersey, M. A. Davis, H. J. Patrick, M. LeBlanc and K. P. Koo, "Fiber Grating Sensors,"

Journal of Lightwave Technology, vol. 15, no. 8, pp. 1442-1463, 1997.

[50]   J. Thrasher, S. Williams, P. Takahashi and J. Sousa, "Pulsed Plasma Thruster Development Using A Novel HAN- Based Green Electric Monopropellant," in *52nd AIAA/SAE/ASEE Joint Propulsion Conference*, Salt Lake City, UT, USA, 2016.

[51]   S. Igarashi, Y. Matsuura, K. Hatai and H. Ikeda, "Safe 0.5N Green Monopropellant Thruster for Small Satellite Propulsion Systems," in *AIAA Propulsion and Energy Forum*, Indianapolis, 2019.

[52]   S. Igarashi, Y. Matsuura, H. Ikeda, T. Nagata and K. Hatai, "0.5 N Thruster for Small Satellite Propulsion System Using HAN/HN-Based Safe Green Monopropellant HNP225," in *Space Propulsion Conference 2020+1*, Virtual, 17-19 March 2021.

[53]   R. Masse, R. A. Spores, S. Kimbrel, M. Allen, E. Lorimor and P. Myers, "GPIM AF-M315E Propulsion System," in *51st AIAA/SAE/ASEE Joint Propulsion Conference*, Orlando, FL, 2015.

[54]   M. Wilhelm, M. Negri, H. Ciezki and S. Schlechtriem, "Preliminary tests on thermal ignition of ADN-based liquid monopropellants," *Acta Astronautica,* vol. 158, pp. 388-396, 2019.